

Slow dynamic elasticity at short timesSangMin Lee ¹ and Richard L. Weaver ^{2,*}¹*Department of Civil and Environmental Engineering, University of Illinois, Urbana, Illinois 61801, USA*²*Department of Physics, University of Illinois, Urbana, Illinois 61801, USA*

(Received 22 November 2023; accepted 6 May 2024; published 7 June 2024)

It has been reported that slow dynamic nonlinear elastic relaxations, widely thought to proceed universally in proportion to the logarithm of time after cessation of mechanical conditioning, actually recover with a smaller slope at early times, with a time of transition that varies with the grain size of the material. This would constitute a heretofore unreported failure of the claimed universality, while suggesting application to nondestructive evaluation and structural health monitoring. Here, we present further observations at short times, in the single bead system, in cement paste, mortar, concrete, sandstone, and granite. Within the limits imposed by finite-duration ring-down such that the effective instant of conditioning cessation is imprecise, and the corresponding ambiguity as to the time at which relaxation begins, we find no reliable sign of such a transition, even in samples of large grain-size mortar and concrete similar to those described elsewhere as having clear and late cutoffs.

DOI: [10.1103/PhysRevE.109.065002](https://doi.org/10.1103/PhysRevE.109.065002)**I. INTRODUCTION**

Slow dynamic elasticity (SD) is a remarkable and universal nonclassical nonlinear elastic behavior in which a modest mechanical conditioning induces a loss of stiffness that afterwards recovers, slowly, like $\log(\text{time})$. This apparent healing after damage is seen in many materials, on length scales from the laboratory to the seismic, and on timescales from milliseconds to years. Laboratory applications of minor strain lead to immediate drops in elastic modulus that then slowly recover [1–9] over seconds to hours. Loss of stiffness and slow recovery are seen also in seismic wave speed near a fault after an earthquake [10–12], where recoveries are monitored over periods from days to years. SD is observed in natural rocks, concrete, and mortar [13,14], and in buildings [15,16].

Materials with simpler chemistry and structure show the effect as well. Cracked glass exhibits the behavior [17–19]. It is seen in unconsolidated aggregates of beads [20–23]. It is seen in an isolated bead confined between plates [24,25]. The inference is that unconsolidated materials replace slow dynamic processes at the internal intergrain contacts of rocks with processes taking place at bead contacts.

Its apparent universality is intriguing, appearing as it does across a variety of materials and structures and having no intrinsic timescales. But, it also receives attention because of its relevance to rock mechanics in general, to earthquake triggering [20], and to ultrasonic materials evaluation [13,14] and structural health monitoring [15,16].

There remains no consensus as to the mechanisms responsible. It has been hypothesized [22] that there is connection to the better-studied phenomenon of $\log(t)$ aging of static friction [26] for which it is argued that contact areas and stiffness between grains will be dominated by asperities. If

the contact areas grow like $\log(t)$, as they do in certain models of plastic flow [26] and as has been observed [27] in careful measurements, one derives $\log(t)$ aging of frictional strength, and presumably also elastic stiffness. It is also thought that moisture may play a role in SD, as it does in the linear elastic moduli of rocks. Bittner [17] reported a strong humidity dependence of SD in cracked glass. A role for moisture was further suggested by Bouquet *et al.*'s observation [28] of $\log(t)$ aging and humidity dependence of the strength of a sand pile against avalanching.

A recurring hypothesis is the Arrhenius, in which recovery proceeds [1,28–30] by way of bond formation after thermally activated barrier penetration, as in Ref. [28] in which the bonds are water bridges, or by way of thermally activated plastic flow [29,30]. The Arrhenius hypothesis explains [30–32] $\log(\text{time})$ aging by hypothesizing a distribution of barrier energies that is constant over a short range. Logarithmic aging over many decades in time requires only constancy of that distribution over a short range in energy. Amir *et al.* [30] pointed out that a relaxation process that is the product of several subprocesses with random rates will also tend to exhibit $\log(\text{time})$ behavior.

Until recently it has been understood that laboratory-measured recoveries, when plotted vs the log of the time since conditioning cessation, are linear from several seconds to hours. Using dynamic acousto-elastic testing (DAET) [33] recent work [8] has reported smaller, or even zero, slopes at the earliest of times (put differently, the relaxation spectrum is weaker for the fastest rates), thus introducing nonuniversal material timescales with transitions at different characteristic times in different materials. Kober *et al.* [34] found that larger grain sizes were associated with more severe, and later, rolloffs. They reported spectral rolloffs as late as several seconds in some concretes. Gueguen *et al.* [16] reported slope diminishment in granite at times as late as several seconds. These are important observations, as they challenge

*Corresponding author: r-weaver@illinois.edu

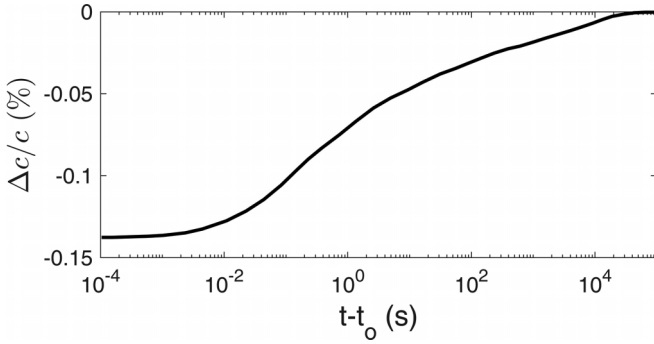


FIG. 1. The data from Shokouhi *et al.*'s [8] Fig. 2 showing slow recovery of ultrasonic wave speed c in Berea sandstone after vibration conditioning. Diminished and zero slope at early times is evident. Their reference time t_0 was chosen 20 ms after the conditioning vibrations were interrupted (15 ms after they appeared to have finished dying away). That choice safely excluded all times before complete cessation of the ring-down of the conditioning but as argued and illustrated here was excessively late, thereby leading to the apparent diminished slope.

universality and suggest other methods for material characterization and Nondestructive Evaluation (NDE), and perhaps point to mechanisms. Figure 1 illustrates the deviation reported by Shokouhi *et al.* [8].

Lobkis and Weaver [9] also reported deviations from log linearity at early times. Unlike those [8,34,16] cited above, they reported *increased* logarithmic slope at short times, discernible in cement paste for $3 < t < 50$ ms and in sandstone for $3 < t < 300$ ms.

That diminished slopes at early times have not been more widely observed has been attributed [8,34] to a dearth of experiments that can access sufficiently short times. The NRUS technique (nonlinear resonant ultrasound spectroscopy), in which changing stiffness is monitored by observing changing resonant frequency [1], does not lend itself well to tracking rapid changes or to fine time resolution; NRUS measurements have typically been confined to times greater than 10 s.

Short-time deviations from $\log(t)$ at milliseconds to seconds may be perplexing for those who ascribe to the Arrhenius hypothesis. This hypothesis holds that the relaxation rates are given by an atomic-scale attack rate of order $\nu = 10^{12}/\text{s}$, but diminished by the need to overcome high barrier energies E through rare thermal fluctuations. Assuming a distribution $f(E)$ of barrier energies, where k is Boltzmann's constant, T is temperature, and C is any convenient measure of wave speed or modulus, one obtains

$$C(t) = C_\infty - \int f(E) \exp(-\nu t \exp(-E/kT)) dE \quad (1)$$

This implies an approximate local relation [32]:

$$dC/d \ln t = kT \langle f(kT \{\ln \nu t + 0.577\}) \rangle. \quad (2)$$

The brackets indicate a smooth running average over a range $\Delta \ln t = \pm 1.28$ [32]. Thus, the hypothesis leads to log linearity when f is constant over a short range in energy. The hypothesis replaces the mystery of log linearity over decades in time (say from 1 to 1000 s) with a lesser mystery of constant f over a short range in E (from 0.69 to 0.86 eV). By the same token,

however, a slope $dC/d \ln t$ that significantly deviates from a constant, as in Fig. 1, requires $f(E)$ to vary significantly over small fractions of an eV. Such is not impossible, but arguably odd.

An equivalent expression [31], obtained by defining $\tau = \exp(E/kT)/\nu$, writes the recovering quantity $C(t)$:

$$C(t) = C_\infty - \int A(\tau)/\tau \exp(-t/\tau) d\tau, \quad (3)$$

in terms of a relaxation spectrum $A(\tau) = kT f(kT \ln \nu \tau)$. Some (e.g., Ref. [34]) define relaxation spectrum as $F(\tau) \equiv A(\tau)/\tau$. Inasmuch as different relaxation times τ could be associated with different microstructural features, sizes, or mechanisms, it could be worthwhile to retrieve the spectrum A . The inverse process of obtaining $A(\tau)$ from the recovery profile $C(t)$ is, however, poorly posed, although it can be facilitated [8,34] by restricting the allowed forms for $A(\tau)$, or it may be approximated by appealing to (2).

Deviations of C from log linearity at short times could be ascribed to features in A at low τ . Such deviations [8,34,16] deserve further inquiry. This paper is intended to address that need. It is well appreciated [31] that the finiteness of (3) at $t = 0$ requires diminished A at short τ . The concern here is whether that necessary cutoff occurs at the timescales reported lately (tens of milliseconds to seconds) or if the cutoff occurs far sooner—as might be expected from the Arrhenius picture.

The next four sections present our measurements of SD recoveries at early times in prisms of Berea sandstone, mortar, concrete, and granite. The data show that ring-down of the conditioning pump vibrations can complicate the analysis. Prolonged ring-down will obscure identification of effective start times t_0 for recovery; it can also contaminate the measurements themselves. Regardless, however, of the associated ambiguities, we shall find that the data exclude early-time deviations from log linearity for times later than a few ms unless t_0 is set implausibly late, i.e. after the pump vibrations have died away.

The provocative 2005 report by Lobkis and Weaver [9] of increased slopes at short times in sandstone and cement paste after impulsive pumping is then discussed and reanalyzed in Sec. VI. We find no evidence for decreased slope at short times.

Section VII presents a study of SD in the single aluminum bead, with focus on the early times. Again, we find that slope diminishment can be excluded, in this case for all times greater than 27 ms.

The tests reported here are confined to 100 s (350 s in Sec. VII) after conditioning, and do not address deviations from linearity that may occur at late times.

We conclude in Sec. VIII with a summary of the evidence and recommendations for further investigation.

II. BEREA

The test system for measurements on the prisms is shown in Fig. 2. It resembles that of the DAET (Dynamic Acousto-Elastic Testing) method [8,33] but differs in two minor ways. The pump conditioning is applied by a Labworks' ET-126-4 electromagnetic shaker (rather than a piezoelectric disk) that is driven at a steady alternating-current amplitude I ,

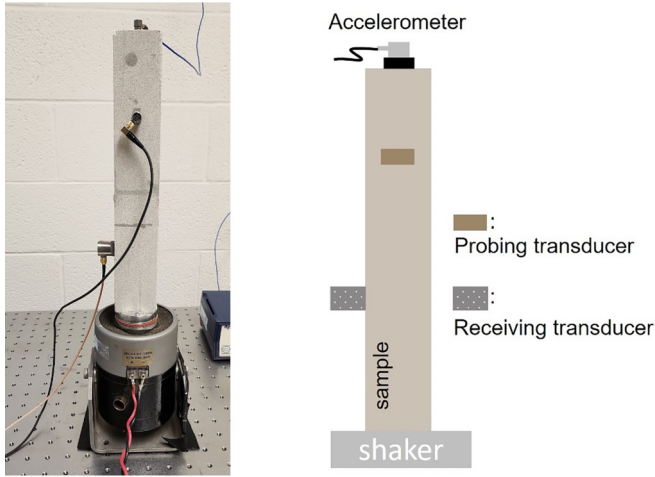


FIG. 2. The laboratory system for studying SD in a prism of rock or mortar. The photo is of the Berea. The sample is attached to the shaker head, and the transducers to the sides, through a removable phenyl salicylate glue.

corresponding to force amplitudes αI with $\alpha = 6.8$ N/A. It is driven longitudinally at fixed frequencies of order 2 to 12 kHz not necessarily on a structural resonance. The resulting vibrations of the sample are monitored by an accelerometer on the tip.

The state of the material is probed using pulse (receive) ultrasonics. Typically DAET [33] tracks the changing transit time, of order $6 \mu\text{s}$, of ballistic ultrasound across a sample. We instead monitor a (~ 500 kHz) diffuse wave that reverberates in the sample with a lifetime of order $500 \mu\text{s}$ (different in different materials) corresponding to path lengths of up to 1 m. The transducers are placed approximately one-quarter vibration wavelength below the top, where the vibration strain is greatest, but they do not face each other. The dilation, or “stretch” of the received waveform, relative to a reference waveform, is equivalent to the fractional wave-speed change $\delta c/c$ reported by others. Signal processing was described at greater length by Yoritomo and Weaver [23]. Ultrasonic pulses are launched with a 320-Hz repetition rate, fast enough to give good time resolution yet slow enough to avoid overlap between successive waveforms. (Waveforms in Berea had durations of order 0.5 ms.) Ultrasound and acceleration signals are acquired continuously and simultaneously at 5 MSA/s for 100 s by a single multichannel CSE8442 PC DAQ board, all channels sharing the same clock. Possible timing error “inter-channel skew” between pump and probe signals are judged to be at most a few nanoseconds.

Our block of Berea sandstone, grain size 125–350 μm , has dimensions $a \times b \times L = 35 - 37 \times 47 - 50 \times 305$ mm. Its lowest free-free natural frequency is $f_1 = 3.42$ and 2.95 kHz (obtained, respectively, from a tap test and first resonance under harmonic forcing in the configuration of Fig 2) From this it is calculated to have a bar wave speed $(\text{Young's modulus/density})^{1/2} = c_{\text{bar}} = 2Lf_1 = 2090$ m/s.

Figure 3 shows the response of the Berea sample upon conditioning with harmonic vibrations at 2.5 A (17 N) for 10 s at 3 kHz. Ultrasonic probe pulses were launched every 3.1 ms, the signal from each resulting diffuse wave being

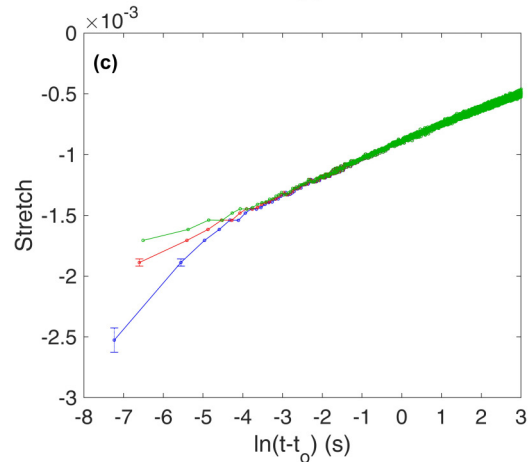
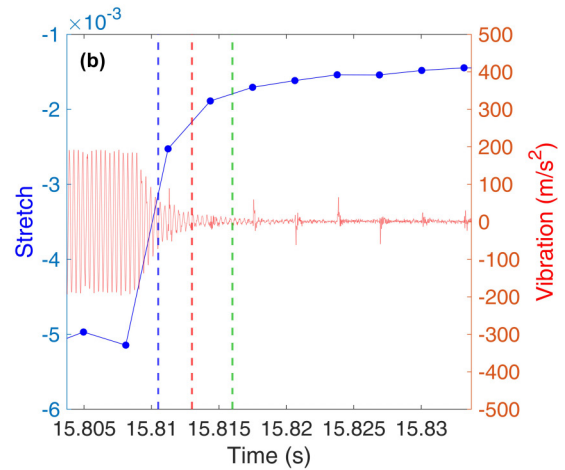
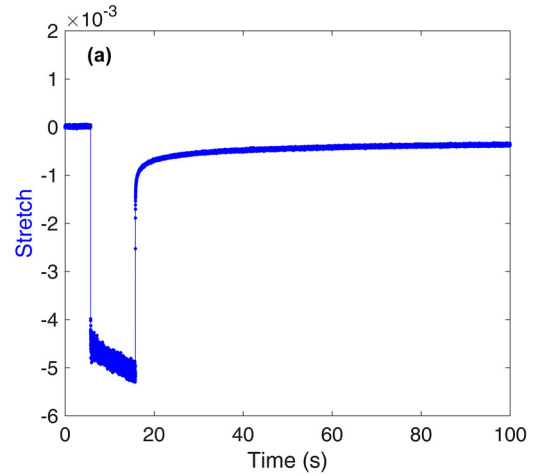


FIG. 3. Behavior of the Berea sample. (a) Plot of stretch $S(t)$ before and after 10 s of conditioning by 3-kHz vibrations with a peak amplitude of $5.5\text{-}\mu\text{s}$ strain. (b) A closeup of the stretches (discrete blue dots) and tip acceleration (continuous red line) near the time of vibration cessation. Dashed lines indicate three choices for t_0 . The periodic blips in the acceleration curve are due to electronic cross talk from the ultrasound. (c) Plots of stretch vs $\ln(t - t_0)$ for the three choices of t_0 .

cross correlated against a reference waveform to calculate the stretch values. Figure 3(a) shows the resulting stretches (blue dots) over the 100 s of record. Each is assigned a time stamp corresponding to the beginning of the waveform, inducing a

timing error of at most 0.25 ms, or half the waveform duration. Figure 3(b) shows both the stretch and the acceleration in the vicinity of conditioning cessation at $t = 15.8$ s. Figures 3(a) and 3(b) call for several remarks:

(1) During the conditioning [between $t = 5$ and 15 s in Fig. 3(a)] the diffuse waveform stretch, representing fractional change in ultrasonic wave speed, drops quickly at first to about -0.005 , and then continues to drop but more slowly. During the conditioning the stretch shows something that looks like noise (but is not—as can be seen by comparing with the low noise level for $t < 5$ s, i.e., before the pump is turned on). The apparent noise is due to classical fast nonlinearity and has a variation that rarely exceeds ± 0.00025 , or $\pm 5\%$ of mean stretch -0.005 . The magnitude of this “noise” would be diminished if the probe waveform had a duration sufficient to average over one or more cycles of the pump, (at a cost of decreased time resolution.) Its noisy appearance is due to random-phase differences between the pump waveform and the ultrasonic pulses.

(2) The acceleration record [continuous red curve in Fig. 3(b)] has a steady-state amplitude of $a_{ss} = 190 \text{ m/s}^2$ and exhibits no obvious sign of higher harmonics. We infer a strain amplitude $a_{ss}/c_{\text{bar}}\omega = 4.8 \mu\text{s}$ strain at a point one-quarter wavelength (equal here to 174 mm) below the tip. Higher harmonics appear at higher driving force (not shown).

(3) Figure 3(b) shows that the pump wave appears to decay exponentially after the signal to the shaker is cut off, with a time constant of about 2 ms.

(4) Figure 3(b) shows three choices, given by the vertical dashed lines, for the reference times t_0 used to construct $\log(t - t_0)$. The earliest is at the time at which the conditioning strain amplitude has dropped to $1/e$ of its steady state of 190 m/s^2 . This occurs about 1.8 ms after the power to the shaker is cut off (dark-blue dashed line). Another is near the $1/e^2$ point of the exponential decay (light-red line about 2 ms later). A third (faint green line) is 4 ms later yet, after the pump vibrations have nearly died away.

(5) There are two distinct and subtle issues related to the choice of t_0 . One is to recognize that any measurements of instantaneous (albeit averaged over the duration of the probe wave) modulus, wave speed, or stretch can be contaminated by fast nonlinearities associated with any simultaneous conditioning. The strength of this contamination to the stretches of interest can be estimated from how severely stretches fluctuate while conditioning is steady. The contamination can be mitigated by rejecting, or flagging as unreliable, any stretches pertaining to times while ring-down still has significant amplitude. One way to do this in a plot vs $\log(t - t_0)$ is to choose a t_0 well after the ring-down—one that will naturally reject all data points where $\log(t - t_0)$ is undefined. This can have the unfortunate consequence of artificially generating a rolloff. But, one need not use a late t_0 to enforce the rejections. It suffices to recognize and quantify any uncertainties in measured stretches. The uncertainty of a measure of stretch at a time t may be calculated from the observed variation while the conditioning was steady, times the ratio of the conditioning amplitude $\bar{a}(t)$ at time t to the amplitude a_{ss} while in the steady state; in this case, $U(t) = \pm 0.00025 [\bar{a}(t)/a_{ss}]$ proportional to the amplitude \bar{a} of the acceleration at t . (We assume these fast nonlinearities are due to leading-order linear

dependence of stiffness on strain.) As the ring-down dies away, this uncertainty vanishes. For these data, the uncertainties are negligible except for the points at stretch $= -0.0025$ and -0.00189 , where they are $U = \pm 0.1$ and $\pm 0.03 \times 10^{-3}$, respectively. These U are reflected by error bars in Fig. 3(c).

(6) A more complex issue is the unknown process by which, during ring-down, ongoing conditioning is competing with ongoing recovery. In plots vs $\log(t - t_0)$ we would like the plots to reveal material properties, and so t_0 should be a time after the cessation of the conditioning and before the beginning of recovery. Yet, during ring-down we surely have both simultaneously and there is no such t_0 ; the best one can do is argue for some range of plausible effective t_0 . Absent a generally accepted theory that describes this domain of simultaneous damage and healing, we can nevertheless examine a set of plausible effective t_0 , and ask what deviations from log linearity would be consistent or inconsistent with that set.

Figure 3(c) plots the stretches vs $\ln(t - t_0)$ for the three choices of t_0 . [35] The upper green line corresponds to the most delayed choice for t_0 , at 15.816 s. As in Ref. [8], this choice saves the green curve from contamination by fast nonlinearity; none of its points suffers from significant uncertainties U . The choice does, however, lie well after the cessation of conditioning and the presumed beginning of any relaxation, so the slope diminishment in the green curve should not be taken as reflecting material properties.

We can quantify any curve’s report of a timescale for early-time slope diminishment by quoting the value of $t - t_0$ at which the slope is half what it is at later times. If we do this for the implausible upper green curve we estimate that time to be earlier than $\exp(-6) = 2.5$ ms.

The red (middle) curve of Fig. 3(c) corresponds to an intermediate and more plausible choice for t_0 . Its first data point has stretch $S = -1.89 \times 10^{-3}$, with an uncertainty $\pm 0.03 \times 10^{-3}$. All of its other points have negligible uncertainty. The red curve runs through the middle of that error bar and shows no curvature. The point at which its slope could be half that at later times is not identifiable but is judged to be no later than $\exp(-6.5) = 1.5$ ms. Replacing the S value with the highest value consistent with the uncertainty does not significantly alter that conclusion.

The lower blue curve of Fig. 3(c) shows, regardless of the uncertainties, increased slope (per $\ln t$) at short times.

We conclude that no plausible choice for t_0 or adjustments in stretches S consistent with their uncertainties U , can support any time of half slope later than 1.5 ms. The bound rises to 2.5 ms if one is willing to accept the implausible choice for t_0 . This is in contrast to the report of Ref. [8]; see Fig 1, of a time of half slope equal to about 20 ms, but it is consistent with a private communication from Jan Kober of $\delta c(t)$ in Berea [34], in which, using a resonance tracking method for velocity changes δc , they found . no rolloffs at times greater than 600 ms. Kober *et al.* [34] had no data from earlier than 600 ms, as that probe method was ill suited to investigating shorter times. They also used a different method to probe stiffness changes, and converted those to an effective relaxation spectrum $F(\tau)$ by inverting Eq. (3). We can reconstruct their δc data by integrating Eq. (3) using the $F(\tau)$ data from their Fig. 4; this

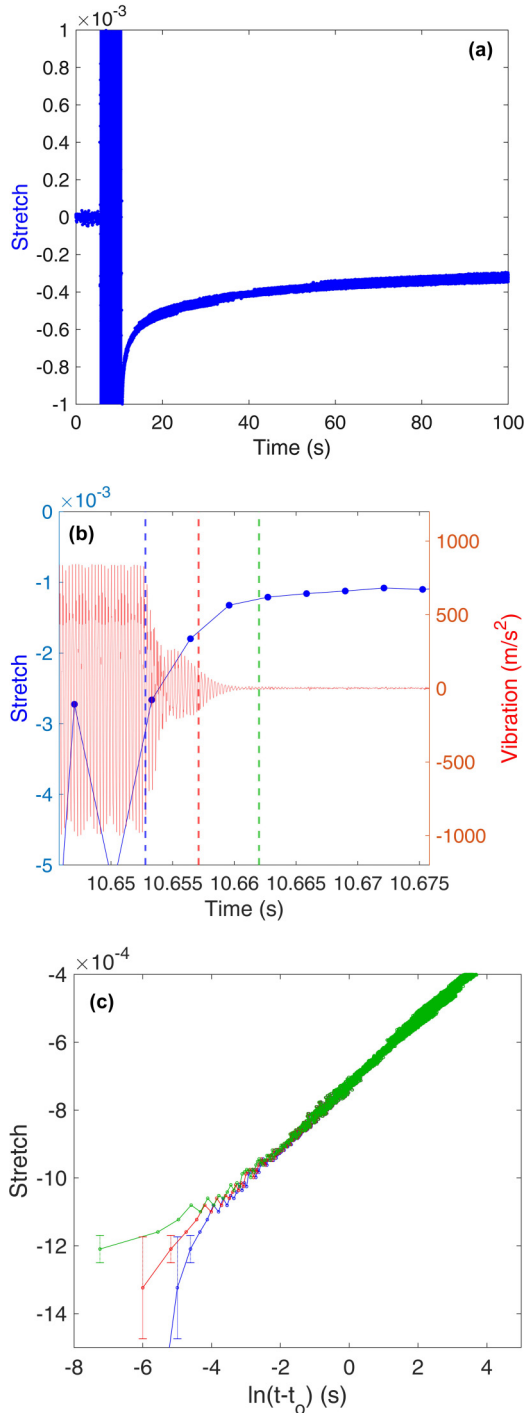


FIG. 4. Slow dynamics in a sample of 2.36 ~ 4.75 – mm grain-size mortar. (a) Stretches before during and after 5 s of 3.8-kHz, 2.8-A conditioning. (b) A closeup of the stretches (discrete blue dots) near the time of vibration cessation, together with the bar’s tip acceleration (continuous red curve). Dashed lines indicate three choices for t_0 . (c) The stretch data for the mortar prism of (a), vs $\ln(t - t_0)$ for the three choices of t_0 .

gives a time of half slope (half the maximum slope) at about 50 ms, far greater than the 2.5-ms bound reported here.

To summarize, inasmuch as there exists a plausible choice (e.g., that of the red middle curve) for t_0 that leads to no

early-time curvature, the data are consistent with there being none. Curvature does appear if one makes implausibly late choices for t_0 (the upper green curve), but even if one accepts that t_0 , the resulting curvature is weaker and occurs much earlier than reported elsewhere.

Sections III–V present three more DAET-like measurements of SD recoveries, one in a mortar prism, one in a concrete prism, and one in granite. For the mortar and concrete samples, the grain size ranged from 2.36 to 4.75 mm and from 4.75 to 9.5 mm, similar to but slightly finer than in the concrete samples of Kober *et al.* [34] (3 to 7 mm and 5 to 15 mm). We find no slope diminishment consistent with those reported there. Similarly, our tests in granite show no discernible curvature, unlike that reported in Ref. [16].

III. SLOW DYNAMICS IN A MORTAR PRISM

A moderate grain-size mortar prism of dimensions 25.4 × 25.4 × 295 mm was constructed consisting of water and Portland Limestone cement (type II) and sand in a ratio by weight of 0.5 : 1 : 3. Sand was sieved to a range of 2.36 ~ 4.75 mm, somewhat finer than Kober *et al.*’s Conc-X04 with a range of 3 to 7 mm. Our sample was initially cured at 100% relative humidity and 25 °C for 2 weeks, followed by an additional 2 weeks of curing at 50% and 25 °C. Samples like this are of particular interest, as Kober *et al.* reported their stronger deviations from log linearity in this kind of material.

The experimental system and procedures are like those used for the Berea discussed above and illustrated in Fig. 2. The sample was epoxied to an aluminum disk (phenyl salicylate glue being judged inadequate for this weaker material) that was then bolted to the shaker head. (This means of mounting was also used for the concrete and granite samples.) The pulse repetition rate was again 320 Hz. Ultrasound waveforms had durations of order 0.8 ms, short enough to avoid overlap between successive pulses.

The sample was driven by 2.8 A (19 N) at 3.8 kHz near the first resonance. Figure 4(a) shows the full history of the evolving stretch for the 5 s before conditioning, the 5 s during conditioning, and the 90 s of recovery.

The absolute noise level is about the same as in Berea (Fig. 3). Signal-to-noise ratio is lower, which is attributed to the mortar having weaker slow dynamics while the noise in stretch is unchanged. The acceleration signal [continuous red curve in Fig. 4(b)] shows the bar to be in a periodic, but not harmonic, steady state due to a classical fast nonlinearity not present in Fig. 3(b).

The points in Fig. 4(b) at stretch = -1.8 and -2.7×10^{-3} (where $t = 10.656$ and 10.653 s, respectively) are likely well contaminated by the dying away vibrations. The large fluctuations in stretch during steady-state conditioning between 5 and 10 s in Fig. 4(a), notwithstanding the much lower conditioning amplitude during ring-down near $t = 10.655$, imply that these data points are too uncertain to be included in further analysis. They are therefore excluded from Fig. 4(c).

The point with $S = -1.32 \times 10^{-3}$ is calculated to have uncertainty $U = \pm 1.7 \times 10^{-4}$; the next point at $S = -1.2 \times 10^{-3}$ has $U = \pm 0.4 \times 10^{-4}$. These U are portrayed with error bars in Fig. 4(c). Other data points have much smaller U , and error bars for them are not portrayed.

As above, we find that the choice of t_0 affects the plots vs $\ln(t - t_0)$. A claim of early-time slope diminishment can only be sustained if one chooses the implausible latest t_0 (upper green curve). Even then the resulting half-slope point occurs only for $t - t_0 < \exp(-5) = 7$ ms.

Seven milliseconds is far earlier than the corresponding time we calculate for the half-slope point (at about 2 s) for Kober *et al.*'s [34] sample Conc-X04 having mean grain size 5 mm (slightly larger than ours). This estimate was obtained by performing the integration, Eq. (3), on the data $F(\tau)$ from Kober *et al.*'s Fig. 4.

The test was repeated after a heat treatment to the sample (90 °C for 12 h). The heat treatment led to a slower ring-down, and though the conditioning strain amplitude was half as much, the SD slope was doubled. Conclusions about recovery rollofs were unaltered.

IV. CONCRETE

A concrete sample was cast using the same materials as the above section's mortar, except that the aggregate was sieved to 4.75 ~ 9.5 mm. Constituent mass ratios and the curing method were the same as in Sec. III. The sample was wider (25.4 × 56 × 290 mm). The grain size of this concrete sample was between Kober *et al.*'s Conc-X04 (grain size 5 ± 2 mm) and Conc-B06 (gravel size 10 ± 5 mm) [34]. All mortar and concrete tests were performed at least 2 months after casting to minimize changes in material properties due to hydration or drying.

The free-free longitudinal fundamental resonance frequency was measured to be 5805 kHz, so the bar wave speed was calculated to be 3367 m/s. When the sample was mounted on the shaker, the resonance frequency reduced to about 4.5 kHz.

The same experimental system, shown in Fig. 2, was used. The sample was driven at 4.3 kHz near the first resonance in the mounted state with 23.8 N (3.5 A). The same 320-Hz ultrasound probe pulse repetition rate was used. Ultrasound waveforms had durations of order 2ms.

Figure 5(a) shows the stretch values before, during, and after 5 s of conditioning and also shows the stretch's relaxation after the conditioning.

Figure 5(b) shows the acceleration signal measured at the tip of the sample, and the stretch, near the time of conditioning cessation. The peak acceleration was measured as 1022 m/s² and the estimated strain level was 11.2 microstrain. Conditioning ring-down was slightly slower than in the mortar case. The time to decay by a factor of e^2 after the shaker turned off was 5.4 ms, slower than the 4.1-ms time observed for the mortar case. Vertical lines indicate three choices for t_0 .

Figure 5(c) plots the relaxing stretches vs $\log(t - t_0)$ for the three choices for t_0 . The points at $S = -2.6$, -2.0 , and -1.75×10^{-3} have uncertainties $U = 1.9$, 0.25 , and 0.05×10^{-3} , respectively, that are indicated by error bars. The lower blue curve shows an increased slope at an early time, and corresponds to choosing t_0 too early, specifically at the time of shaker off [see Fig. 5(b)]. This conclusion survives consideration of uncertainties. The upper green curve, displaying a decreased slope at an early time, represents the choice of t_0 being implausibly [see Fig. 5(b)] late. If one

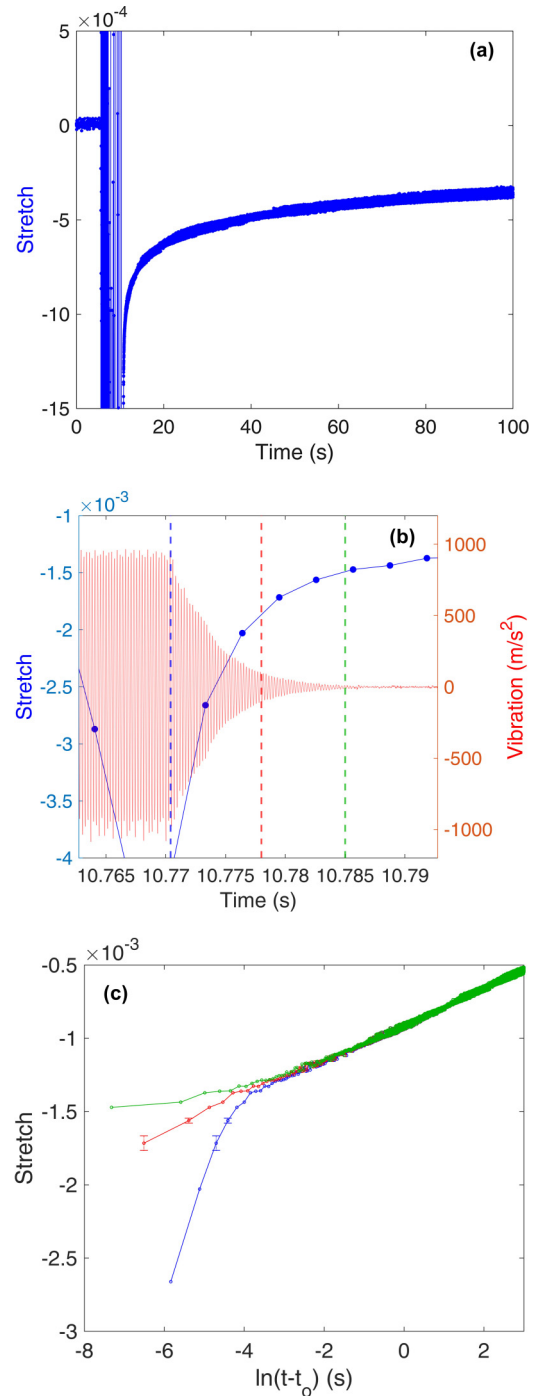


FIG. 5. Slow dynamics in the concrete prism having grain size 4.75 ~ 9.5 mm. (a) Stretches before, during, and after 5 s of conditioning at 4.3 kHz and 3.5 A. (b) A closeup of stretch data (discrete blue dots) near the time of vibration cessation, together with the tip acceleration (continuous red curve). Three choices for t_0 are indicated. (c) The stretch data for the concrete prism of (a), plotted vs $\ln(t - t_0)$ for the three choices of t_0 .

accepts this t_0 and corresponding curve regardless, one might identify a half-slope time at about $\exp(-5.5) = 4$ ms. The middle and more plausible (red) curve shows no curvature down to $t = \exp(-6.5) = 1.5$ ms. This behavior is inconsistent with that reported by Kober *et al.* [34], for whom

Conc-X04 had a half-slope point at 2 s, and Conc-B04 at about 4 s.

V. GRANITE

Similar tests were conducted on a block of Rockville Granite with dimensions of $27.2 \times \{25.1 \sim 26.6\} \times 104$ mm and mass of 194 g. This rock was primarily composed of quartz and plagioclase with some biotite. The average grain size and the largest grain size were 10 and 20 mm, respectively.

Based on the free-free longitudinal resonance test with an impactor, the fundamental longitudinal resonance frequency was found to be 20.35 kHz, allowing us to estimate the bar wave speed as 4249 m/s.

The small height of this sample and the frequency-range limitations of our shaker precluded driving the sample near resonance. The strength of the shaker nevertheless permitted development of sufficient conditioning strain to see SD. The test configuration was otherwise the same as for Berea, mortar, and concrete. Figure 6 show the response using the same pulse repetition rate of 320 Hz. Waveform duration in the granite sample was 1 ms, so there was no overlap between successive ultrasonic waveforms.

Figure 6(a) illustrates the stretch response over 100 s. The data collection started with 5 s of reference data followed by 5 s of conditioning with a 27-N harmonic forcing at 7.5 kHz. The remaining 90 s was dedicated to examining the SD relaxation.

Figure 6(b) shows the stretch and acceleration at the tip of the sample near the end of the conditioning. The conditioning ring-down was substantially faster here, and less exponential in character, than in other tests. The nonexponential character was ascribed to the presence of harmonics induced by fast nonlinearities. The time to decay by a factor of e^2 after the shaker switch is turned off was only 0.8 ms, which may be compared to 3.8, 23, and 4.1 ms for the Berea sandstone, single bead, and mortar cases, respectively.

Figure 6(c) plots the stretches vs $\ln(t - t_0)$ for the three choices of t_0 illustrated in Fig. 6(b). Again, the upper green curve pertains to the latest choice for t_0 , and the lower blue curve to the earliest. Uncertainties were calculated as in other sections and found to be, for the three points with $S = -1.5 \times 10^{-3}$ and the three points with $S = -1.4 \times 10^{-3}$, respectively, $U = \pm 0.1 \times 10^{-3}$ and $\pm 0.04 \times 10^{-3}$. The point at $S = -2.1 \times 10^{-3}$ had very large $U = \pm 1.0 \times 10^{-3}$ and was therefore excluded from further consideration. The points at $S = -1.5$ and -1.4×10^{-3} had sufficient uncertainties U that permitted a hypothesis of diminished slope at short times with times of transition $t < \exp(-5) = 7$ ms. This was severely at odds with reports of transition times in granite of order 1 s, as reported elsewhere [16].

VI. SD IN CEMENT PASTE AND SANDSTONE AFTER IMPACT

In Secs. II–V slow dynamics was examined for a variety of blocklike specimens using the modified DAET illustrated in Fig 2, in which pump conditioning was imposed by vibrations and evolving wave speed was probed using diffuse field ultrasonics. It is worthwhile to explore alternative measurements of

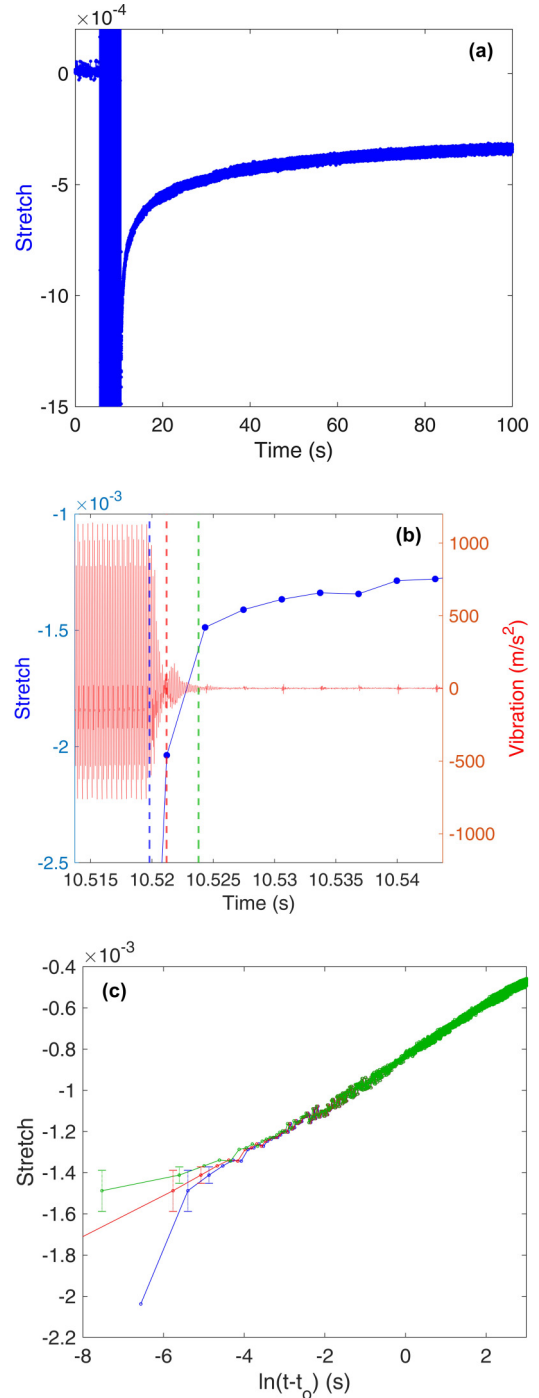


FIG. 6. Slow dynamics in the Rockville granite conditioned by 7.5-kHz harmonic vibrations with a peak amplitude of 1100 m/s^2 measured at the tip of the sample. (a) Stretch values before during and after 5 s of conditioning. (b) A closeup of the stretches (discrete blue points) near the time of vibration cessation, together with the sample's tip acceleration (continuous red curve.) Three choices for t_0 are indicated by vertical dashed lines. (c) The stretches vs $\ln(t - t_0)$ for the three choices of t_0 .

SD as well; are conclusions affected? In this section we revisit an older report in which the pump was a high strain impact and the specimen's changing Larsen frequency was used as a

probe. In the following section early-time SD was studied in the single-bead configuration.

The earliest work to report slow dynamics at short times was that of Lobkis and Weaver [9] for blocks of cement paste and sandstone, with examined times from 3 ms to 400 s, over 5 decades in time. Conditioning was provided by the impact of a wooden ball bearing, the acoustic emission from which provided the time of impact accurate to within microseconds. Elastic stiffness changes were assessed by monitoring a 525-kHz Larsen frequency (the steady-state harmonic screech provided by an ultrasonic version of the familiar audio feedback screech heard when microphones and speakers are too close and/or gain is too high.) The SD recoveries were found to be linear in $\log(t)$ for late times. Signs of deviation (with increased slope) from linearity in $\log(t - t_{\text{impact}})$ were apparent for times between 3 and 50 ms in cement paste, and between 3 and 135 ms in sandstone. See the lower curves of Figs. 7(a) and 7(b).

Our study of accelerated recovery (per $\log t$) at short times is in apparent contrast with reports elsewhere [8,16,34] of lower slope (per $\log t$) at short times. For this reason further inquiry is especially interesting. Was the observation [9] meaningful?

It is not clear that the time of impact t_{impact} corresponds to the end of significant conditioning and beginning of recovery. The sample surely vibrated for some time after the impact. The end of conditioning is therefore at some time at or after the impact. We can replot the data of Ref. [9] using various guesses for t_0 . Figures 7(a) and 7(b) show the results of that operation.

Figure 7(a) shows four curves corresponding to four choices for t_0 . The bottom blue curve is that plotted by Lobkis and Weaver [9], with reference time taken at the instant of ball impact. Increased slope at short times is evident. The lower-middle red curve is for a reference time t_0 5 ms later; the upper-middle green for 10 ms after the impact; the top black for 20 ms after the impact. The data indicate that, if one is willing to entertain a time 5 or 10 ms after impact as the effective moment at which conditioning ceases and recovery begins, then there is little or no sign of deviation from log linearity. One must choose an even later t_0 if short-time diminished slope [8,16,34] is to be asserted.

We would like to know which of these t_0 , if any, best describes an effective end of conditioning and beginning of recovery. To inform that judgment, the wooden ball was dropped on the original cement paste sample, and the resulting vibrations detected with an accelerometer. That signal was high-pass filtered at 600 Hz and integrated to give material velocity. See Fig. 8. The envelope rises sharply at the impact and then decays, initially with a time constant of order 2 ms. But, a low-frequency wave persists for many tens of milliseconds. Conditioning could in principle continue beyond the time of impact, due to the stresses during these vibrations. It is difficult to judge the relative strength of conditioning due to the impact (with large strain but confined to short duration and extent, estimated [9] as of order 1%, tens of microseconds, and 300 μm , respectively) and the longer-lasting lesser strain (well below 1- μs strain in Fig. 8) in the more extended reverberant vibrations. Setting t_0 to 5 ms after impact is perhaps reasonable. Setting it at 20 ms, necessary for

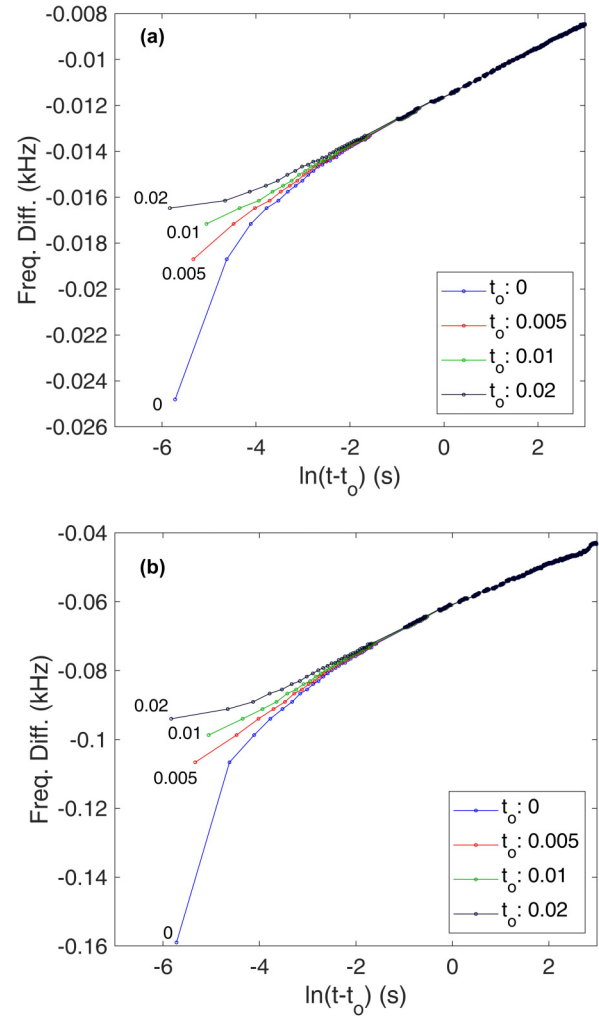


FIG. 7. Color online Slow dynamics after impact conditioning by a 4-mm wooden ball on (a) a cement paste prism and (b) a sandstone prism. Data from Ref. [9]. Different choices for t_0 (in seconds after ball impact) result in different curves. We remark that the lower blue curves' first points correspond to a time only 3 ms after the impact, and is arguably contaminated by classical fast nonlinearities from the impact's acoustic emission ring-down (see Fig. 8). One might also argue that the continuous Larsen wave time averages over the impact's oscillations and is therefore not sensitive to leading-order fast nonlinearities.

Fig 7(a)'s upper curves' diminished slopes, would demand admitting the long-lived very low amplitude as a significant agent of conditioning. This we think unlikely. We conclude that there is no good argument for short-time slope diminishment, and some uncertain evidence for a steepening.

Figure 7(b) is like 7(a) except that it corresponds to Lobkis and Weaver's [9] sandstone sample. The conclusions are unaltered. In particular, a reference time choice 5 or 10 ms after impact again serves to remove early-time deviations from log linearity.

Perhaps the chief lesson to be taken from this is that impact conditioning is problematic; it can generate low-frequency reverberant strains whose slow decay obscures identification of a reference time t_0 . It is also noteworthy that impact pump

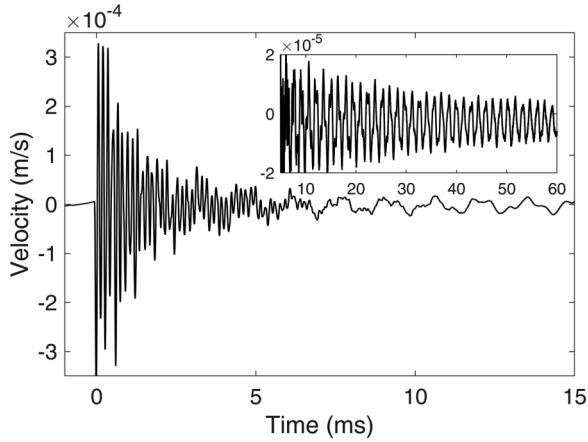


FIG. 8. Accelerometer response (after high-pass filtering and time integration) to the impact of a 4-mm-diameter wooden ball on the cement bar of Lobkis and Weaver [9]. Signal decays quickly over the first few ms, but a low-amplitude 700 to 1700-Hz component persists for much longer. The strains associated with these material velocity v are estimated using $\varepsilon = v/c_{\text{bar}}$ [36] to be very small, of order 10 to 100 nanostrain.

strains of order 1% [9] are far greater than are typical in the SD literature; one may speculate that the unusual steepening at short time is a consequence.

VII. EARLY TIME IN SINGLE BEADS

Figure 9 shows the system for measuring SD in a single bead. The structure sits on vibration isolation and optical tables to minimize the influence of ambient building vibrations. An ET-126-4 electromagnetic shaker also sits on that table and provides 500-Hz conditioning vibrations, typically for 20 s. An accelerometer placed on the upper slab over the bead reports amplitudes of order 1 m/s^2 while the shaker is on and provides a proxy for the dynamic conditioning force on the bead. The bead–slab contact stiffness is diminished by the vibrations, but then recovers after the conditioning ceases. Ultrasonic pulses are introduced to the upper slab at rates up to 16 Hz. If it were faster, the diffuse wave from one pulse might overlap that from the next. (Waveform durations are 20 to 30 ms.) The resulting diffuse field leaks into the lower slab via the bead, whose transmissibility is dominated by the stiffness of its contacts. When that stiffness diminishes, the diffuse

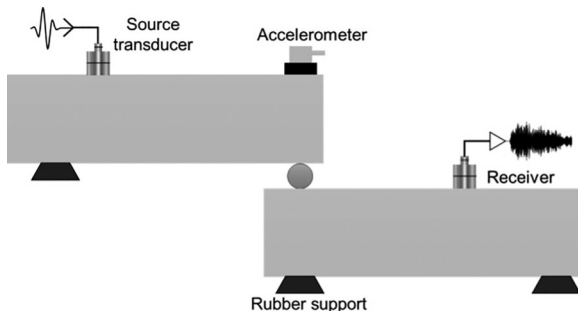


FIG. 9. The single-bead experiment (not to scale).

signal in the lower slab is delayed. Coda wave interferometric methods extract that delay.

For the single-bead tests, the pump (accelerometer) and probe (ultrasound) signals are acquired by separate digitizers. The accelerometer signal is acquired by the built-in PC audio-in channel at a sampling rate of 11 kSa/s. The diffuse ultrasound signal is acquired at 10 MSa/s by the PC-DAQ board used in the previous sections. To correct for potential timestamp differences between the two digitizers, the trigger-out pulse from the PC-DAQ board, which signals the beginning of ultrasound acquisition, is used to trigger the analog ultrasound pulser. It is also acquired by the built-in audio-frequency digitizer when the accelerometer signal is not being collected (i.e., before and after conditioning). Comparison of the timestamps of the ultrasound waveforms (captured by the PC-DAQ board) and the trigger-out pulse (captured by the audio-in channel) reveals a difference having fluctuations of $\pm 0.5 \text{ ms}$ on a test-specific mean of 10 to 13 ms. The mean is then used to adjust the timestamps for plots like Fig. 10(b) of Y and acceleration to assure their synchronization. Timing errors are thereby judged to be below $500 \mu\text{m}$ and negligible for the present purposes.

This system, with pulse-repetition rates of order 1 Hz, was first introduced by Yoritomo and Weaver [24,25]. Weaver and Lee [37] discussed the theory relating measurements of delay to stiffness changes. They also [32] investigated the effect of dynamically heating the bead. Throughout that work, $\log(t)$ recoveries were routinely observed, and with low noise. But, their slow pulse-repetition rate of 1 Hz, now improved, prevented investigation of the behavior at the shortest times.

Figure 10(a) plots the diffuse wave delays Y in a system consisting of an aluminum bead and slabs. Ninety seconds of reference data are followed by 20 s of conditioning and 340 s of recovery. Average delays during conditioning are obscured by rapidly varying large positive and negative “noise,” due to fast nonlinear dynamics similar to that seen in Figs. 3(a), 4(a), 5(a) and 6(a). Vibrations cease between $t = 108.8$ and 108.9 s , after which the bead is left with a diminished stiffness. The stiffness then recovers, quickly at first and then increasingly slowly. Timestamps for the delays Y have been set at the midpoint of the 10-ms segment of the received diffuse waveforms used to calculate delays Y . Figure 10(b) presents the same data on an expanded scale in the vicinity of the vibration cessation time. It also shows the accelerometer signal (continuous red curve) whose 500-Hz vibrations do not cease instantaneously, but ring down with a time constant of about 15 ms. Three choices for reference time t_0 are indicated by the vertical dashed lines.

Figure 10(c) plots the delays Y vs $\log(t - t_0)$ for the three choices of t_0 . The upper green curve is for the most delayed of the three choices, $t_0 = 127 \text{ ms}$ after the beginning of the ring-down. It shows a diminishment of slope at short times reminiscent of that reported elsewhere [8]. But, its t_0 is manifestly long after the conditioning has ended, so its diminishing slope should not be considered a material property but rather an artifact of the late choice for t_0 . Should one nevertheless accept the late t_0 and green curve, one would report a diminishment in slope at early times, with a half-slope point well less than 50 ms.

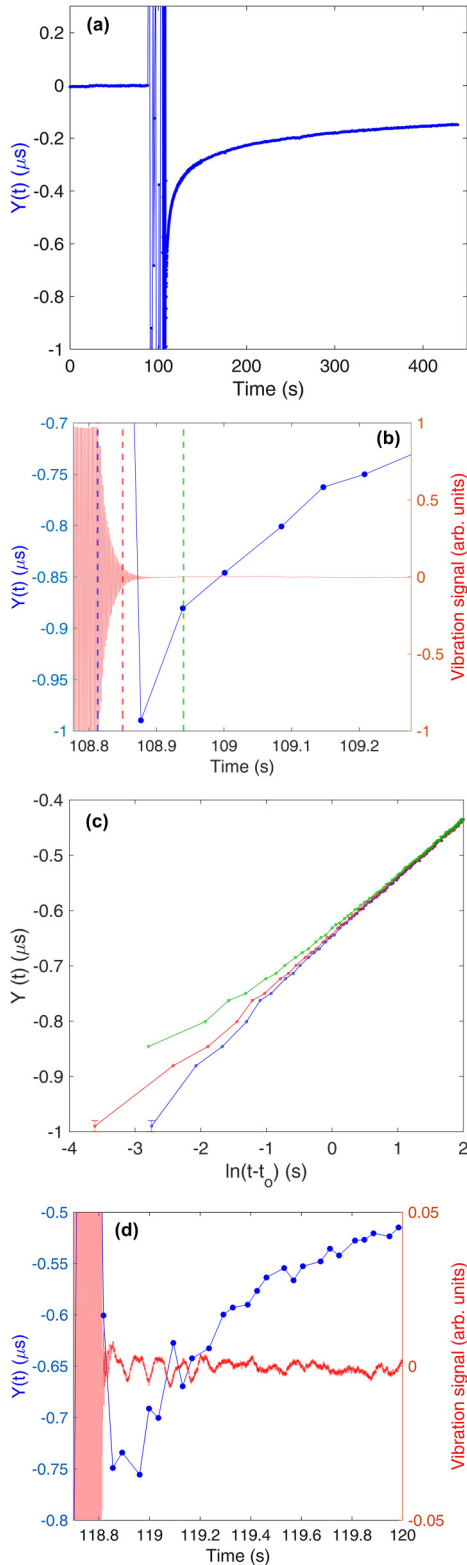


FIG. 10. Slow dynamics in a single aluminum bead confined between two slabs (Fig. 9). (a) Ultrasonic delays Y in the transmitted probe wave before, during, and after 20 s of conditioning. (b) Behavior in the vicinity of the cessation of conditioning. Three choices for t_0 are indicated. (c) The stretches are plotted vs log time for the three choices of t_0 . (d) The same measurement in a glass structure for which long-lasting ~ 10 -Hz vibrations contaminate the early-time recovery.

The middle red curve shows good linearity down to its limit at $\exp(-3.6) = 27$ ms.

The blue curve is based on another not very plausible choice for t_0 (at the very beginning of the ring-down). It shows a slightly increased slope at short times. The net conclusion is that these data do not support diminishments in slope for any transition times later than 27 ms.

These conclusions are unaffected by the uncertainty $U = \pm 6$ ns of the point at $Y = -0.99$ μs .

Figure 10(d) shows data from a similar test on a single glass bead and slabs. Residual ~ 10 -Hz vibrations of unknown origin noticeably contaminate the measured delays with fast nonlinearities. Positive and negative excursions of the delays Y correlate with negative and positive values of the acceleration signal at late times. The contaminations sufficiently corrupt the early-time data that conclusions are limited; plots vs $\ln(t)$ (not shown) indicate only that diminished slope, if any, must be confined to times before 100 ms. We do not consider this case further.

VIII. SUMMARY AND CONCLUSIONS

We have examined the earliest times of slow dynamic recovery in a variety of materials. This includes concrete, mortar, Berea, and granite, in which significant early-time rolloffs, as late as seconds, have been reported by others. We also examined early times in a single-bead system and reexamined an old study of SD in cement paste and sandstone under impact conditioning. In every case we found that there was a plausible choice for effective reference time t_0 that led to no early-time diminishment in recovery slope, even down to accessible timescales as low as milliseconds. The data are therefore consistent with the hypothesis of no slope diminishment. The converse hypothesis (that there is a diminished slope at short times greater than a few ms) is consistent with the data only if one chooses an implausibly late t_0 . In such cases, however, the measured curvature was weak, with transition times below or of the order of 2 to 7 ms (27 ms in the single-bead case, where slow ring-down prevents inference of a tighter bound), far below those transition times of order 1 s reported by others.

While there are differences in material and samples and protocols, both in pumping and probing, between these tests and others in the literature, the 2-to-3 orders-of-magnitude discrepancies seem larger than can be explained by such considerations. We mention two of those differences:

The choice of reference time t_0 is critical. The later the reference time, the more the plots vs $\log(t - t_0)$ will curve upward (i.e., exhibit a diminished slope and later transition time). The diminished slopes seen in Fig. 1 may be ascribed to its analysis's excessively late choice for t_0 . But, an excessively late choice of t_0 will not explain the discrepancy with Kober *et al.* [34], who chose t_0 at the moment of the electronic cutoff to the conditioning. Were we to have made the same choice, all our curves, i.e., like the lower curves in Figs. 3(c), 4(c), 5(c), and 6(c), would curve down, with increased slope at earliest times.

Kober *et al.* conditioned their samples with longitudinal vibrations for 5 min at tens of kilohertz, in the vicinity of a resonance. They then probed, using their protocol I, with

a low-amplitude continuous sinusoid at the same frequency, and monitored the phase and amplitude of the sinusoidal response to extract the wave speed. This process is very different from ours. We condition for a shorter period using vibrations and probe with higher-frequency pulsed ultrasound, extracting wave-speed changes by means of coda-wave interferometry. It is an interesting speculation to attribute the differences in early-time SD to differences in measurement protocols. An anonymous reviewer has suggested that conditioning duration might be critical, or even that conditioning might be continuing to the times t_0 judged here as implausibly late.

Further explorations of SD at early times would benefit from varying pump protocols. Greater attention to more rapid decay of the pump conditioning would limit the time range over which fast nonlinearities contaminate the measurements, and limit the range of plausible choices for t_0 . We also imagine that theoretical tools with which to analyze periods of

simultaneous conditioning and recovery could mitigate the reference time ambiguities.

In sum, our measurements fail to reproduce the material-dependent early-time cutoffs reported elsewhere [8,16,34] but rather support the original notion that SD relaxations do not depend on material details, have no timescales, and are universal. They thereby degrade hopes that measuring such timescales could aid in nondestructive materials evaluation. Clarification of the early-time behavior may aid in identifying microphysical mechanisms.

ACKNOWLEDGMENTS

The authors are grateful to J. Popovics, R. Makhnenko, and N. Bondarenko for providing samples, and to J. Kober for providing the data for Ref. [34]’s Figs. 1 and 4. This material is based upon work supported by the U.S. Department of Energy, Office of Science, Office of Basic Energy Sciences, under Award No. DE-SC0021056.

-
- [1] J. Ten Cate, E. Smith, and R. Guyer, Universal slow dynamics in granular solids, *Phys. Rev. Lett.* **85**, 1020 (2000).
 - [2] J. Ten Cate and T. J. Shankland, Slow dynamics in the nonlinear elastic response of Berea sandstone, *Geophys. Res. Lett.* **23**, 3019 (1996).
 - [3] E. Smith and J. Ten Cate, Sensitive determination of nonlinear properties of Berea sandstone at low strains, *Geophys. Res. Lett.* **27**, 1985 (2000).
 - [4] J. Ten Cate, Slow dynamics of earth materials: An experimental overview, *Pure Appl. Geophys.* **168**, 2211 (2011).
 - [5] R. A. Guyer and P. A. Johnson, Nonlinear mesoscopic elasticity: Evidence for a new class of materials, *Phys. Today* **52**(4), 30 (1999).
 - [6] P. A. Johnson and A. Sutin, Slow dynamics and anomalous fast dynamics in diverse solids, *J. Acoust. Soc. Am.* **117**, 124 (2005).
 - [7] R. A. Guyer and P. A. Johnson, *Nonlinear Mesoscopic Elasticity* (John Wiley and Sons, 2009).
 - [8] P. Shokouhi, J. Riviere, R. Guyer, and P. A. Johnson, Slow dynamics of consolidated granular systems: Multi-scale relaxation, *Appl. Phys. Lett.* **111**, 251604 (2017).
 - [9] O. I. Lobkis and R. L. Weaver, On the Larsen effect to monitor small fast changes in materials, *J. Acoust. Soc. Am.* **125**, 1894 (2009).
 - [10] D. P. Schaff and G. C. Beroza, Coseismic and postseismic velocity changes measured by repeating earthquakes, *J. Geophys. Res.-Solid Earth* **109**, B10302 (2004).
 - [11] F. Brenguier, M. Campillo, C. Hadziioannou, N. Shapiro, and E. Larose, Postseismic relaxation along the San andreas Fault at Parkfield from continuous seismological observations, *Science* **321**, 1478 (2008).
 - [12] M. Gassenmeier, C. Sens-Schonfelder, T. Eulenfeld, M. Bartsch, P. Victor, F. Tilmann, and M. Korn, Field observations of seismic velocity changes caused by shaking-induced damage and healing due to mesoscopic nonlinearity, *Geophys. J. Int.* **204**, 1490 (2016).
 - [13] M. Scalerandi, C. Mechri, M. Bentahar, A. Di Bella, A. S. Gliozzi, and M. Tortello, Experimental evidence of correlations between conditioning and relaxation in hysteretic elastic media, *Phys. Rev. Appl.* **12**, 044002 (2019).
 - [14] N. Tremblay, E. Larose, and V. Rossetto, Probing slow dynamics of consolidated granular multicomposite materials by diffuse acoustic wave spectroscopy, *J. Acoust. Soc. Am.* **127**, 1239 (2010).
 - [15] A. Astorga, P. Guéguen, and T. Kashima, Nonlinear elasticity observed in buildings during a long sequence of earthquakes, *Bull. Seismol. Soc. Am.* **108**, 1185 (2018).
 - [16] P. Gueguen, M.-A. Brossault, P. Roux, and J. C. Singaicho, Slow dynamics process observed in civil engineering structures to detect structural heterogeneities, *Eng. Struct.* **202**, 109833 (2020).
 - [17] J. A. Bittner, Understanding and predicting transient material behaviors associated with mechanical resonance in cementitious composites, Ph.D. thesis, University of Illinois, 2019.
 - [18] J. A. Bittner and J. S. Popovics, Direct imaging of moisture effects during slow dynamic nonlinearity, *Appl. Phys. Lett.* **114**, 021901 (2019).
 - [19] V. Zaitsev, V. Gusev, and B. Castegnede, Thermoelastic mechanism for logarithmic slow dynamics and memory in elastic wave interactions with individual cracks, *Phys. Rev. Lett.* **90**, 075501 (2003).
 - [20] P. A. Johnson and X. Jia, Nonlinear dynamics, granular media and dynamic earthquake triggering, *Nature (London)* **437**, 871 (2005).
 - [21] V. Zaitsev, V. Gusev, V. Tournat, and P. Richard, Slow relaxation and aging phenomena at the nanoscale in granular materials, *Phys. Rev. Lett.* **112**, 108302 (2014).
 - [22] X. Jia, T. Brunet, and J. Laurent, Elastic weakening of a dense granular pack by acoustic fluidization: Slipping, compaction and aging, *Phys. Rev. E* **84**, 020301 (2011).
 - [23] J. Y. Yoritomo and R. L. Weaver, Slow dynamic nonlinearity in unconsolidated glass bead packs, *Phys. Rev. E* **101**, 012901 (2020).
 - [24] J. Y. Yoritomo and R. L. Weaver, Slow dynamics in a single glass bead, *Phys. Rev. E* **101**, 012902 (2020).

- [25] J. Y. Yoritomo and R. L. Weaver, Slow dynamic elasticity in unconsolidated metal structures, *Phys. Rev. E* **102**, 012901 (2020).
- [26] T. Baumberger and C. Caroli, Solid friction from stick–slip down to pinning and aging, *Adv. Phys.* **55**, 279 (2006).
- [27] J. H. Dieterich and B. D. Kilgore, Direct observation of frictional contacts: New insights for state-dependent properties, *Pure Appl. Geophys.* **143**, 283 (1994).
- [28] L. Bouquet, E. Charlaix, S. Ciliberto, and J. Crassous, Moisture-induced ageing in granular media and the kinetics of capillary condensation, *Nature (London)* **396**, 735 (1998).
- [29] A. V. Lebedev and L. A. Ostrovsky, A unified model of hysteresis and long-time relaxation in heterogeneous materials, *Acoust. Phys.* **60**, 555 (2014).
- [30] A. Amir, Y. Oreg, and Y. Imry, On relaxation and aging of various glasses, *Proc. Natl. Acad. Sci. USA* **109**, 1850 (2012).
- [31] R. Snieder, C. Sens-Schonfelder, and R. Wu, The time dependence of rock healing as a universal relaxation process, a tutorial, *Geophys. J. Int.* **208**, 1 (2016).
- [32] R. L. Weaver and S. M. Lee, Slow dynamics in a single bead with mechanical conditioning and transient heating, *Phys. Rev. E* **107**, 044902 (2023).
- [33] G. Renaud, J. Riviere, P. -Y. Le Bas, and P. A. Johnson, Hysteretic nonlinear elasticity of Berea sandstone at low-vibrational strain revealed by dynamic acousto-elastic testing, *Geophys. Res. Lett.* **40**, 715 (2013).
- [34] J. Kober, A. S. Gliozzi, M. Scalerandi, and M. Tortello, Material grain size determines relaxation-time distributions in slow-dynamics experiments, *Phys. Rev. Appl.* **17**, 014002 (2022).
- [35] All three curves hint at slight late-time diminishment in slope. This interesting behavior is outside the scope of the current effort.
- [36] This estimate follows from equating time- and space-averaged kinetic and strain energies.
- [37] R. L. Weaver and S. M. Lee, Diffuse energy transport and coda-wave interferometry for resonant transmission between reverberant structures, *J. Acoust. Soc. Am.* **150**, 830 (2021).